Ligand K-Edge X-ray Absorption Spectroscopy as a Probe of Ligand−Metal Bonding: Charge Donation and Covalency in Copper−Chloride Systems

Susan E. Shadle,[†] Britt Hedman,[*,‡] Keith O. Hodgson,[*,†,‡] and Edward I. Solomon[*,†]

Department of Chemistry and Stanford Synchrotron Radiation Laboratory, Stanford University, Stanford, California 94305

Received March 31, 1994[⊗]

X-ray absorption spectra (XAS) have been measured at the chloride K-edge for a series of complexes containing chloride ligands bound to open shell d^9 copper ions in order to probe ligand−metal bonding. The intensity of the pre-edge feature in these spectra reflects the covalency in the half-occupied $d_{x^2-y^2}$-derived molecular orbital (HOMO) of the complex. The energy of the pre-edge feature is related to both the charge on the ligand and the HOMO energy. An analysis of the intensity and energy of the pre-edge feature as well as the energy of the rising absorption edge provides quantitative information about the covalency of the ligand−metal interaction, the charge donated by the chloride, and the energy of the copper d-manifold. The results demonstrate that ligand K-edge XAS features can be used to obtain information about ligand−metal bonding. The results also identify the chemical basis for trends in the XAS data for the following complexes: D_{4h} $CuCl_4^{2-}$, D_{2d} $CuCl_4^{2-}$, planar *trans*-$CuCl_2(pdmp)_2$ (pdmp = *N*-phenyl-3,5-dimethylpyrazole), square pyramidal $CuCl_5^{3-}$, the planar dimer $KCuCl_3$, the distorted tetrahedral dimer $(Ph_4P)CuCl_3$, and two dimers with mixed ligation, one containing a bridging chloride, and the other, containing terminally bound chloride. Several of these results are supported by independent spectral data or by basic ligand field concepts. A geometric distortion from square planar to distorted tetrahedral results in a decrease in the chloride−copper HOMO covalency but an increase in the total charge donation by the chlorides. While the geometry can maximize the overlap for a highly covalent HOMO, this does not necessarily reflect the overall charge donation. The Cl−Cu(II) bonding interactions are dependent on the nature of the other coordinating ligands. Replacement of chlorides by less strongly donating ligands causes an increase in charge donation by the remaining chloride ligands. An increase in the coordination number of the copper or in the charge donation by the ligands (resulting in a lower effective nuclear charge on the copper) causes an increase in the copper d-manifold energy. Finally, the bonding of a terminal *vs* bridging chloride is very different, in that for the latter there is more total charge donation and a higher ligand covalent contribution to the HOMO of the two coppers.

Introduction

Insight into the electronic structure of an absorbing atom can be obtained from an analysis of X-ray absorption edge spectra.[1,2] This has been demonstrated for transition metal centers such as Cu, Fe, Ni, and Mo at the metal K-edges.[3−6] It has also recently been shown that absorption edges of ligands such as S and Cl can be used to probe the electronic structure of transition metal complexes[7−9] and metalloprotein active sites.[7,9] The K-edges of these atoms fall in the 2−3 keV range in which spectral features are well-resolved.[10] Further, for ligands such as S and Cl the 3p orbitals are directly involved in bonding with transition metal ions. Because the electric dipole-allowed transitions for K-edges are 1s → *n*p, ligand K-edge X-ray absorption spectroscopy provides a direct probe of these ligand−metal bonding interactions.

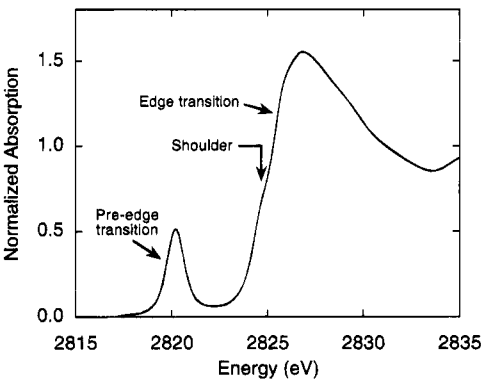

Figure 1. Pre-edge and edge regions of a typical Cl K-edge absorption spectrum for a Cl bound to an open shell metal ion. (Shown here is the Cl K-edge for Cs_2CuCl_4). Shown are the intense, well-resolved pre-edge feature, the main edge transition, and a shoulder which occurs on the rising edge.

* To whom correspondence should be addressed.
† Department of Chemistry, Stanford University.
‡ Stanford Synchrotron Radiation Laboratory, Stanford University.
⊗ Abstract published in *Advance ACS Abstracts,* August 15, 1994.

(1) Heald, S. M.; Tranquada, J. M. In *Physical Methods of Chemistry*; Rossiter, B. W.; Hamilton, J. F., Eds.; John Wiley & Sons: New York, 1990; Vol. 5; pp 189−272.
(2) Bianconi, A. In *X-ray Absorption: Principles, Applications, Techniques of EXAFS, SEXAFS, and XANES*; Koningsberger, D. C.; Prins, R., Eds.; John Wiley & Sons: New York, 1988; pp 573−662.
(3) Kau, L. S.; Spira-Solomon, D. J.; Penner-Hahn, J. E.; Hodgson, K. O.; Solomon, E. I. *J. Am. Chem. Soc.* **1987**, *109*, 6433−6442.
(4) Roe, A. L.; Schneider, D. J.; Mayer, R. J.; Pyrz, J. W.; Widom, J.; Que, L. *J. Am. Chem. Soc.* **1984**, *106*, 1676−1681.
(5) Eidsness, M. K.; Sullivan, R. J.; Scott, R. A. In *Bioinorganic Chemistry of Nickel*; Lancanster, J. R., Jr., Ed.; VCH: Deerfield Beach, FL, 1988; pp 73−92.
(6) Conradson, S. D.; Burgess, B. K.; Newton, W. E.; Hodgson, K. O.; McDonald, J. W.; Rubinson, J. F.; Gheller, S. F.; Mortenson, L. E.; Adams, M. W. W.; Mascharak, P. K.; Armstrong, W. A.; Holm, R. H. *J. Am. Chem. Soc.* **1985**, *107*, 7935−7940.
(7) Hedman, B.; Frank, P.; Gheller, S. F.; Roe, A. L.; Newton, W. E.; Hodgson, K. O. *J. Am. Chem. Soc.* **1988**, *110*, 3798−3805.
(8) Hedman, B.; Hodgson, K. O.; Solomon, E. I. *J. Am. Chem. Soc.* **1990**, *112*, 1643−1645.
(9) Shadle, S. E.; Penner-Hahn, J. E.; Schugar, H. J.; Hedman, B.; Hodgson, K. O.; Solomon, E. I. *J. Am. Chem. Soc.* **1993**, *115*, 767−776.
(10) The high energy resolution is due to the combined effect of increased core−hole lifetime (Krause, M. O.; Oliver, J. H. *J. Phys. Chem. Ref. Data* **1979**, *8*, 329-338) and improved monochromator resolution.

0020-1669/94/1333-4235$04.50/0

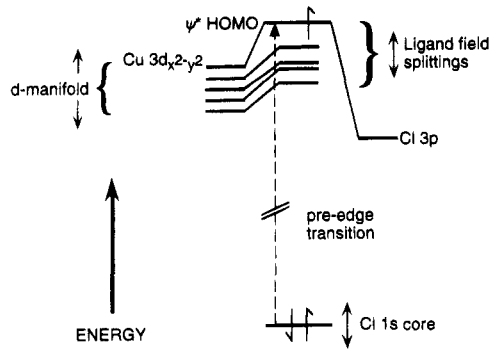

Figure 2. Schematic representation of the contributions to the pre-edge transition energy. The pre-edge energy is determined by shifts both in the Cl 1s core energy and in the energy of the HOMO of the complex. The HOMO energy is determined by overall shifts in the d-manifold related to coordination number and charge on the metal as well as the specific repulsive interaction of the HOMO determined by the ligand field of the complex.

A representative K-edge absorption spectrum for a chloride ligand bound to an open shell cupric d^9 ion is shown in Figure 1. The pre-edge feature well separated from the rising edge is absent in metal systems with a full d-manifold and is assigned as the Cl 1s $\rightarrow$ Cu $3d_{x^2-y^2}$ transition, where the $3d_{x^2-y^2}$ orbital is the half-occupied, highest-occupied molecular orbital (HOMO).[8] Figure 2 shows an energy level diagram depicting the transition which gives rise to the pre-edge spectral feature. Due to the localized nature of the Cl 1s orbital, this transition can have absorption intensity only if the half-occupied Cu 3d orbital contains a significant component of Cl 3p character as a result of covalency. Thus, a more complete description of this transition is Cl 1s $\rightarrow \psi^*$, where $\psi^* = (1 - \alpha'^2)^{1/2}(\text{Cu } 3d_{x^2-y^2}) - \alpha'(\text{Cl } 3p)$, and α'^2 represents the amount of Cl 3p character in the antibonding molecular orbital.[8] The electric dipole intensity observed in this pre-edge transition is simply the intensity of the pure dipole-allowed Cl 1s $\rightarrow$ 3p transition weighted by α'^2 (eq 1). Thus, the pre-edge intensity provides a

$$I(\text{Cl } 1s \rightarrow \psi^*) = \alpha'^2 I(\text{Cl } 1s \rightarrow \text{Cl } 3p) \qquad (1)$$

direct probe of the ligand contribution to the HOMO orbital due to bonding.[8]

As indicated in Figure 2, a combination of factors affect the energy position of a pre-edge transition. A shift in the core Cl 1s energy, which is related to the relative charge on the chloride, results in a change in the observed pre-edge energy. More charge donation to the metal results in a shift to deeper binding energy (*vide infra*). In addition, the energy of the pre-edge transition is affected by the HOMO energy, which has two contributions. First, the geometry of the ligand field of the complex determines the d-orbital energy splitting pattern and thus contributes to the HOMO energy. Second, the overall d-manifold can shift in energy. This is related to both the coordination number of the metal (the total antibonding and repulsive interactions with the ligands) and the effective charge on the metal, which affects the energy of all the metal orbitals.

At higher energy in Figure 1 are absorption edge features due to transitions to bound states higher in energy than the HOMO. The intense electric dipole-allowed transitions which give rise to the main edge jump are Cl 1s $\rightarrow$ 4p transitions. Transitions to molecular orbitals with both Cl 3p and metal (*e.g.*, 4s) character can appear as shoulders on the rising edge. The energy of the main edge transition, which can be determined in some cases from the rising edge inflection point, has been shown to be linearly related to the charge on the absorber.[11-13] The binding energies of core electrons undergo chemical shifts which relate to changes in the valence electron distribution due to bonding. A decrease in positive charge on the Cl will result in the core 1s energy shifting to lower binding energy; delocalization of Cl electron density due to bonding results in a core orbital shift to deeper binding energy. Since the unoccupied Cl 4p orbitals are less effected by charge donation, shifts in the rising edge inflection energy *directly* reflect shifts in the Cl 1s core in response to the effective charge on the atom.

In this study, we utilize the relationship between pre-edge intensity and covalency (eq 1) to further develop the application of pre-edge intensity to quantitate the ligand−metal covalency in transition metal complexes. We also develop a quantitative analysis of the pre-edge and edge energies for ligand K-edge spectra. This analysis, based on the model described above, allows us to quantitatively separate the contributions from both the Cl 1s core and the HOMO shifts to the pre-edge transition energy. The Cl 1s core shift is quantitated from energy shifts in the edge transition. Ligand field contributions to the HOMO energy are determined from optical spectra. Correction of the observed pre-edge energy for these effects allows the contribution to the pre-edge energy from energy shifts of the d-manifold to be determined. In several cases, independent methods confirm the results of this methodology.

This energy and intensity analysis is applied to Cl K-edge absorption spectra for a series of Cl−Cu(II) complexes. This simple ligand−metal system allows us to determine the electronic and geometric structural basis for trends observed in the ligand K-edge spectra. The structural variations which are examined include the distortion of the $CuCl_4^{2-}$ ion from a square planar (D_{4h}) to a distorted tetrahedral (D_{2d}) geometry, the substitution of pyrazoles for two chloride ligands in a square planar complex, and the addition of a fifth ligand to tetrachlorocuprate, generating the square pyramidal $CuCl_5^{3-}$ complex. Studies of planar and tetrahedrally-distorted $Cu_2Cl_6^{2-}$ dimers compare terminal to bridging chlorides in two geometric environments. Also, spectra for dimers which contain square pyramidal coppers coordinated primarily by N/O ligands and either bridging or terminal chloride allow us to easily resolve features of bridging *vs* terminal chlorides which can then be related to systems with both types of chloride involved in bonding.

Experimental Section

A. Sample Preparation. All model compounds were prepared according to published methods: $(\text{creatininium})_2CuCl_4$,[14] Cs_2CuCl_4,[15,16] $CuCl_2$(N-phenyl-3,5-dimethylpyrazole)$_2$,[17] (N(2amet)pipzH$_3$)$CuCl_5$·$2H_2O$) [N(2amet)pipzH$_3$ = (N-(2-ammonioethyl)piperazinium)],[18] $KCuCl_3$,[19] $(Ph_4P)CuCl_3$,[20] [Cu_2(PAP6Me)(OH)Cl_3]·H_2O [PAP6Me = 1,4-bis((6′-methyl-2′-pyridyl)amino)phthalazine],[21] and [Cu_2(L-O$^-$)Cl][BPh_4]$_2$·CH_3-

(11) Ovsyannikova, I. A.; Batsanov, S. S.; Nasanova, L. I.; Batsanova, L. R.; Nekrasova, E. A. *Bull. Acad. Sci. USSR, Phys. Ser. (Engl. Transl.)* **1967**, *31*, 936−940.
(12) Cramer, S. P.; Eccles, T. K.; Kutzler, F. W.; Hodgson, K. O.; Mortenson, L. E. *J. Am. Chem. Soc.* **1976**, *98*, 1287−1288.
(13) Kirby, J. A.; Goodin, D. B.; Wydrzynski, T.; Robertson, A. S.; Klein, M. P. *J. Am. Chem. Soc.* **1981**, *103*, 5537−5542.
(14) Udupa, M. R.; Krebs, B. *Inorg. Chim. Acta* **1979**, *33*, 241−244.
(15) Sharnoff, M. *J. Chem. Phys.* **1965**, *42*, 3383−3395.
(16) McGinnety, J. A. *J. Am. Chem. Soc.* **1972**, *94*, 8406−8413.
(17) Francisco, R. H. P.; Lechat, J. R.; Massabni, A. C.; Melios, C. B.; Molina, M. *J. Coord. Chem.* **1980**, *10*, 149−153.
(18) Antolini, L.; Marcotrigiano, G.; Menabue, L.; Pellacani, G. C. *J. Am. Chem. Soc.* **1980**, *102*, 1303−1309.
(19) Willett, R. D.; Dwiggins, C., Jr.; Kruh, R. F.; Rundle, R. E. *J. Chem. Phys.* **1963**, *38*, 2429−2436.
(20) Textor, M.; Dubler, E.; Oswald, H. R. *Inorg. Chem.* **1974**, *13*, 1361−1365.
(21) Bautista, D. V.; Dewan, J. C.; Thompson, L. K. *Can. J. Chem.* **1982**, *60*, 2583−2593.

$COCH_3$ [(where L-O^- is a binucleating ligand providing two pyridyl nitrogens and a tertiary amine to each Cu and a bridging phenolate oxygen)].[22] The starting material for $[Cu_2(L\text{-}O^-)Cl][BPh_4]_2 \cdot CH_3COCH_3$ was generously provided by Dr. Kenneth Karlin.

For the X-ray absorption experiments, samples were ground into a fine powder (at least several minutes of grinding with mortar and pestle). The powder was dispersed as thinly as possible (to minimize the possibility of self-absorption) on mylar tape containing an acrylic adhesive determined to be free of chlorine contaminants. We have verified that this procedure minimizes self-absorption effects in the data by systematically testing progressively thinner samples until the observed intensity no longer varies with the thickness of the sample. Samples were prepared identically to those in which self-absorption was shown to be negligible. The powder on tape was mounted across the window of an aluminum plate. The $[Cu_2(L\text{-}O^-)Cl][BPh_4]_2 \cdot CH_3COCH_3$ sample was prepared in a dry, inert atmosphere. A polypropylene film window protected the sample from exposure to air.

B. X-ray Absorption Measurements and Data Acquisition Parameters. X-ray absorption data were measured at the Stanford Synchrotron Radiation Laboratory using the 54-pole wiggler beamline 6−2 in low magnetic field mode (5 kG) with a Pt-coated focusing mirror and a Si(111) double crystal monochromator, under dedicated conditions (3.0 GeV, ~50 mA). Some data were measured on beamline X10C at the National Synchrotron Light Source (2.5 GeV, 200 mA). The monochromator was in both cases detuned ~30% to eliminate higher harmonic components in the X-ray beam. Details of the optimization of this setup for low-energy studies have been given in an earlier publication.[7]

The data were collected as fluorescence excitation spectra utilizing an ionization chamber as a fluorescence detector.[23,24] Several (two to three) scans were measured for each sample. The energy was calibrated from the Cl K-edge spectra of Cs_2CuCl_4, run at intervals between the samples. The maximum of the first edge-region feature in the spectrum was assigned to 2820.20 eV. Scans ranged from 2740 to 3100 eV, with a step size of 0.08 eV in the edge region for most samples. Several samples (D_{4h} $CuCl_4^{2-}$, $CuCl_5^{3-}$, and $KCuCl_3$) had a larger pre-edge step size of 0.2 eV. The spectrometer resolution was ~0.5 eV. Calculating and comparing first and second derivatives for model compounds measured during different experimental sessions result in a reproducibility in edge position better than ~0.1 eV for these experiments.

C. Data Analysis. Data were averaged, and a smooth background was removed from all spectra by fitting a polynomial to the pre-edge region and subtracting this polynomial from the entire spectrum. Normalization of the data was accomplished by fitting a flat polynomial or straight line to the post-edge region and normalizing the edge jump to 1.0 at 2840 eV.

The inflection point of the rising edge for each Cl K-edge spectrum was determined from the energy of the maximum of the first derivative of the data in the rising edge region. In spectra in which there were overlapping peaks in the first derivative, the highest energy peak in the rising edge region was used in comparisons.

D. Fitting Procedures. The intensities and energies of pre-edge features were quantitated by fits to the data. The fitting program EDG_FIT, which utilizes the double precision version of the public domain MINPAK fitting library[25] was used. EDG_FIT was written by Dr. Graham N. George of the Stanford Synchrotron Radiation Laboratory. All spectra were fit over the range 2818−2826 eV. Pre-edge features were modeled by pseudo-Voigt line shapes (simple sums of Lorentzian and Gaussian functions). This line shape is appropriate as the experimental features are expected to be a convolution of the Lorentzian transition envelope[26] and the Gaussian line shape imposed by the spectrometer optics.[23,27,28] A fixed 50:50 ratio of Lorentzian to Gaussian contribution for the pre-edge feature successfully reproduced these spectral features.

Functions modeling the background underneath the pre-edge features were chosen empirically to give the best fit. The rising edge was mimicked by combinations of pseudo-Voigt line shapes (of varying admixtures). In some cases a step function was included. The number and positions of the functions used were chosen based on the features evident in the second derivative of the spectrum. In all cases the minimum number of functions required to successfully reproduce the data was utilized.

The second derivative of the data was compared to the second derivative of the fit. In all cases, a number of fits were obtained which reproduced the data and the second derivative. The value reported for the area of a fitted feature (where peak area was approximated by the height multiplied by the full-width-at-half-maximum (fwhm)) is the average of all the pseudo-Voigts which successfully fit the feature. For each sample, the standard deviation of the average of the areas was calculated to quantitate the error. In several cases the second derivative of the data was not of sufficient quality to be used to define the goodness of fit. In these cases, the fits were made only to the data. Because the fit to the second derivative of the data is most sensitive to the fwhm of the fitting function, the fwhm for these samples was stepped through the entire range of values found for the model systems with well-behaved second derivatives. The area and standard deviation reported are from the set of fits produced in this way. In the cases where the pre-edge contained overlapping features, the average area and standard deviation for each feature was determined separately as described above. The standard deviation of these area values was carried through in any analysis which utilized the fitted peak areas.

E. Determination of Rising Edge Positions. The energies reported for the rising edge position were determined from the maximum in the first derivative of the data corresponding the rising edge inflection point. These measurements were performed independently of the above described fitting procedures.

F. Error Analysis. There are several possible sources of systematic error in the analysis of these spectra. Normalization procedures can introduce a 1−3% difference in pre-edge peak heights, as determined by varying the parameters used to normalize a set of Cl K-edge spectra such that the final fits met requirements of consistency. This maximum of ~3% error and the error resulting from the fitting procedure discussed above (section D) were taken into account in the calculation of pre-edge intensities and subsequent determinations of covalency. Experimental self-absorption could, in principle, result in an artificially low observed intensity. However, care was taken to avoid self-absorption in these experiments (*vide supra*), and this effect is assumed to be negligible.

The uncertainty in pre-edge and edge energies is limited by the reproducibility of the edge spectra (better than ~0.1 eV). Thus, relative energies of features are reported with an error of ±0.1 eV. For pre-edge features with overlapping energies, the error in the energy position was determined from fits to the data in the manner described above (section D). The centers of ligand field spectra were used to quantitate energy shifts of HOMO orbitals for complexes with unassigned ligand field spectra. The error in this approximation has been determined to be ~0.2 eV from comparison of the centers of assigned ligand field spectra to the HOMO shift determined from the assigned transitions. It was assumed that there is no error in the HOMO shifts for those determined from assigned ligand field spectra.

Results

Figure 3 shows the Cl K-edge X-ray absorption spectra of the inorganic compounds $NaClO_4$, $KClO_3$, and KCl, as well as the first derivatives of these spectra. The inflection point of the rising edge, determined by the energy of the maximum in the first derivative, ranges over almost 10 eV for this series of

(22) Karlin, K. D.; Farooq, A.; Hayes, J. C.; Cohen, B. I.; Rowe, T. M.; Sinn, E.; Zubieta, J. *Inorg. Chem.* **1987**, *26*, 1271−1280.
(23) Lytle, F. W.; Greegor, R. B.; Sandstrom, D. R.; Marques, E. C.; Wong, J.; Spiro, C. L.; Huffman, G. P.; Huggins, F. E. *Nucl. Instrum. Methods* **1984**, *226*, 542−548.
(24) Stern, E. A.; Heald, S. M. *Rev. Sci. Instrum.* **1979**, *50*, 1579−1582.
(25) Argonne National Laboratory; B. S. Garbow, K. E. Hillstrom, J. J. More.
(26) Agarwal, B. K. *X-ray Spectroscopy*; Springer-Verlag: Berlin, 1979, p 276 ff.
(27) Tyson, T. A.; Roe, A. L.; Frank, P.; Hodgson, K. O.; Hedman, B. *Phys. Rev. B* **1989**, *39A*, 6305−6315.
(28) Lytle, F. W. In *Applications of Synchrotron Radiation*; Winick, H.; Xian, D.; Ye, M. H.; Huang, T., Eds.; Gordon & Breach: New York, 1989; pp 135.

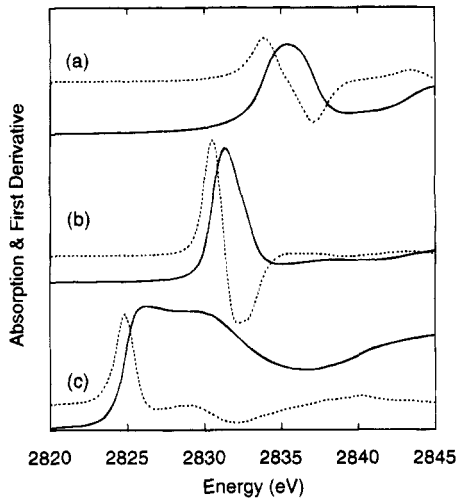

Figure 3. Cl K-edge spectra of (a) $NaClO_4$, (b) $KClO_3$, and (c) KCl. For each spectrum the solid line is the X-ray absorption data and the dashed line is the first derivative of the data. Spectral intensity are rescaled due to a large variation in the *y*-scale of these spectra. The inflection point of the rising edge, determined by the energy of the maximum in the first derivative, ranges over almost 10 eV for this series of complexes. There are no pre-edge features observed in these data.

complexes. The inflection point is lowest for KCl at 2824.8 eV (Figure 3a) and highest for $NaClO_4$ at 2833.7 eV (Figure 3c), while that of $KClO_3$ occurs at 2830.5 eV (Figure 3b). Table 1 summarizes these results as well as all other numerical information presented in the Results.

The Cl K-edge X-ray absorption spectra of the monomeric Cl—Cu(II) complexes D_{4h} $CuCl_4^{2-}$, D_{2d} $CuCl_4^{2-}$, square planar *trans*-$CuCl_2pdmp_2$ (pdmp = *N*-phenyl-3,5-dimethylpyrazole), and square pyramidal $CuCl_5^{3-}$ are shown in Figure 4. Each spectrum exhibits an intense, well-resolved pre-edge feature at lower energy than the edge. The pre-edge feature in the spectrum of D_{2d} $CuCl_4^{2-}$ (Figure 4b) appears at 2820.2 eV. This is at lower energy than in the others, which are 2820.6, 2820.5, and 2820.6 eV for D_{4h} $CuCl_4^{2-}$, $CuCl_2pdmp_2$, and $CuCl_5^{3-}$, respectively.

Figure 4 also shows the first derivative of each spectrum. In contrast to the spectra in Figure 3, the first derivatives shown in Figure 4 reflect structure on the rising edge: a broad maximum or two well-defined maxima in the region of the rising edge. The lower energy feature corresponds to the inflection point of the shoulder seen on the rising edge in each spectrum. The higher energy feature in the first derivative reflects the energy of the inflection point for the Cl 1s → 4p main edge transition. The inflection point of this Cl-based transition is used for comparison and occurs at 2825.0, 2825.3, 2825.3, and 2824.9 eV for D_{4h} $CuCl_4^{2-}$, D_{2d} $CuCl_4^{2-}$, $CuCl_2pdmp_2$, and $CuCl_5^{3-}$, respectively.

Shown in Figure 5 are the Cl K-edge X-ray absorption spectra of the dimeric complexes $KCuCl_3$, $(Ph_4P)CuCl_3$, and (Ph_4P)-$CuClBr_2$. The planar $Cu_2Cl_6^{2-}$ unit in $KCuCl_3$ has tetragonal symmetry at each copper,[19] including two additional Cl^- ligands at ~3.0 Å which belong to the equatorial plane of adjacent binuclear units (Figure 6a). The latter two complexes contain isolated $Cu_2Cl_6^{2-}$ [20] and $Cu_2Cl_2Br_4^{2-}$ [29] units for which the Cu symmetry is distorted T_d (Figure 6b). Studies of the (Ph_4P)-$CuClBr_2$ have shown[29] that the Cl has a preference for the bridging position in the dimer.

The Cl K-edge spectrum of each complex exhibits a pre-edge feature. Compared to the monomers, the pre-edge width at half-height for $KCuCl_3$ (Figure 5a) is significantly larger and the feature is asymmetric. A fit of this spectrum (shown in Figure 5a, inset) reveals two transitions contained in the pre-edge feature envelope. In the spectrum of $(Ph_4P)CuCl_3$ (Figure 5b) the pre-edge is split into two distinct transitions. The pre-edge transition at lower energy is more intense than that at higher energy. The Cl K-edge spectrum of $(Ph_4P)CuClBr_2$ (Figure 5c) also exhibits a split pre-edge feature. The energies are identical to those found in $(Ph_4P)CuCl_3$, but in this spectrum the higher energy transition is more intense. Because some of the Cl^t are replaced with bromides in $CuClBr_2$, the reduction in relative intensity of the lower energy peak requires that it be Cl^t based and the higher energy peak is then assigned as originating from the Cl^b. The Cl^t (lower energy) transition has some residual intensity in $(Ph_4P)CuClBr_2$ because the complex contains some Cl^t.[29] By analogy, the two transitions in $KCuCl_3$ are assigned as the lower energy transition arising from the Cl^t and the higher energy transition arising from the Cl^b. The pre-edge transitions for the tetrahedrally distorted dimers (2820.0 and 2821.0 eV) are shifted to lower energy relative to those in $KCuCl_3$ (2820.6 and 2821.3 eV).

Figure 5 also shows the first derivative of each spectrum. As for the monomers, the derivatives reflect structure on the rising edge. The inflection points of the main edge transitions for $KCuCl_3$ and $(Ph_4P)CuCl_3$ are at 2824.9 and 2825.3 eV, respectively.

Figure 7 shows the Cl K-edge X-ray absorption spectra for the mixed ligated dimers $[Cu_2(PAP6Me)(OH)Cl_3]\cdot H_2O$ (Cu_2-PAP) and $[Cu_2(L\text{-}O^-)Cl][BPh_4]_2\cdot CH_3COCH_3$ ($Cu_2(L\text{-}O^-)Cl$). The Cu_2PAP dimer,[30] shown schematically in Figure 6c, contains square pyramidal five-coordinate coppers bridged by a hydroxyl oxygen in the equatorial plane, and by a chloride at a shared apical position with a large bond distance of >2.6 Å. Each copper is further coordinated by an equatorial terminal chloride, a pyridyl nitrogen and a phthalazine nitrogen in the equatorial plane. The $Cu_2(L\text{-}O^-)Cl$ dimer complex,[22] shown schematically in Figure 6d, contains square pyramidal five-coordinate coppers bridged by a phenolate oxygen and a chloride in the equatorial plane of the square pyramid. Each axial position is occupied by a pyridyl nitrogen, and the remaining equatorial positions for each copper are occupied by one pyridyl and one amine nitrogen. Each Cl K-edge spectrum (Figure 7) exhibits a pre-edge feature, which is at 2820.7 eV for Cu_2PAP and 2821.4 eV for $Cu_2(L\text{-}O^-)Cl$. The first derivatives of the spectra, shown in Figure 7, again reflect the rising edge structure in these systems. The main edge inflection points for these complexes are at 2824.8 and 2825.8 eV for Cu_2PAP and Cu_2-$(L\text{-}O^-)Cl$, respectively.

Analysis

A. Cl K-edges. As described in the Introduction, the intense electric dipole allowed transition observed at the onset of the edge jump is a bound state Cl 1s → 4p transition. The energy of this main edge transition is determined from the rising edge inflection point, and shifts in this energy directly reflect shifts in the Cl 1s core in response to the relative charge on the atom. This correlation between charge and inflection point is clearly observed in the Cl K-edges of $NaClO_4$, $KClO_3$, and KCl (Figure 3). In $NaClO_4$, Cl has a formal charge of +7; in $KClO_3$, it has a formal charge of +5; and Cl in KCl is formally −1. The rising edge inflection points for these complexes at 2833.7,

(29) Estes, W. E.; Wasson, J. R.; Hall, J. W.; Hatfield, W. E. *Inorg. Chem.* **1978**, *17*, 3657–3664.

(30) Mandal, S. K.; Thompson, L. K.; Hanson, A. W. *J. Chem. Soc., Chem. Commun.* **1985**, 1709–1711.

Table 1. Cl K-Edge Transition Energies and Intensities and Spectral Analysis

	Cl K-edge spectral features			Cl K-edge spectral analysis		
complex	pre-edge energy (eV)[a]	normalized pre-edge intensity[b]	rising edge inflection point[c]	calcd charge[d]	renormalized pre-edge intensity[e]	covalency per Cl (%)[f]
$NaClO_4$			2833.7	**1.91**		
$KClO_3$			2830.5	**1.49**		
KCl			2824.8	**−0.87**		
D_{4h} $CuCl_4^{2-}$	2820.6	0.75	2825.0	−0.65	0.76	9.8
D_{2d} $CuCl_4^{2-}$	2820.2	0.57	2825.3	−0.56	0.57	7.3
$CuCl_2pdmp_2$	2820.5	0.76	2825.3	−0.56	0.76	9.7
$CuCl_5^{3-}$	2820.6	0.57	2824.9	−0.69	0.72	9.2
$KCuCl_3$ (Cl^t)	2820.6 ± 0.05	0.66 ± 0.09	2824.9	−0.69	0.99 ± 0.14	12.7 ± 1.8
$KCuCl_3$ (Cl^b)	2821.3 ± 0.09	0.35 ± 0.09	(2825.6)[g]	−0.46	1.05 ± 0.26	13.5 ± 3.5
$(Ph_4P)CuCl_3$ (Cl^t)	2820.0	0.50	2825.3	−0.56	0.74	9.5
$(Ph_4P)CuCl_3$ (Cl^b)	2821.0	0.30	(2826.3)[g]	−0.23	0.92	11.7
$(Ph_4P)CuClBr_2$ (Cl^t)	2820.0					
$(Ph_4P)CuClBr_2$ (Cl^b)	2821.0					
Cu_2PAP	2820.7	0.53	2824.8	−0.72	0.80	10.2
$Cu_2(L\text{-}O^-)Cl$	2821.4	1.07	2825.8	−0.39	1.07	13.8

[a] Reported error is the standard deviation of the energy as determined from fitting of the spectra; the error is ≤0.009 eV unless otherwise noted. [b] Reported error is the standard deviation of the area as determined from fitting of the spectra and the ~3% error from normalization of the data; the error is ≤0.04 unless otherwise noted. [c] Error in the inflection point is <0.1 eV; the inflection point reported is the highest energy feature in the first derivative in the rising edge region. [d] Charge is generated from the relationship determined from Auger spectroscopy which established the charges of $KClO_4$, $KClO_3$, and KCl (the values in boldface type); see Figure 8. [e] Areas are properly normalized to the total chloride which contributes to pre-edge intensity. The reported error is the standard deviation obtained from fits to the data and the ~3% error from normalization of data; error is ≤0.05 unless otherwise noted. [f] Error reported is the standard deviation of the reported covalency value. Error is ≤0.5% unless otherwise noted. Zero error in the 39% total covalency (9.75% per Cl) in D_{4h} $CuCl_4^{2-}$ used to quantitate the pre-edge intensity has been assumed. [g] Inflection point of Cl^b estimated relative to that measured for Cl^t of each complex, utilizing the observed pre-edge energy splitting (see text).

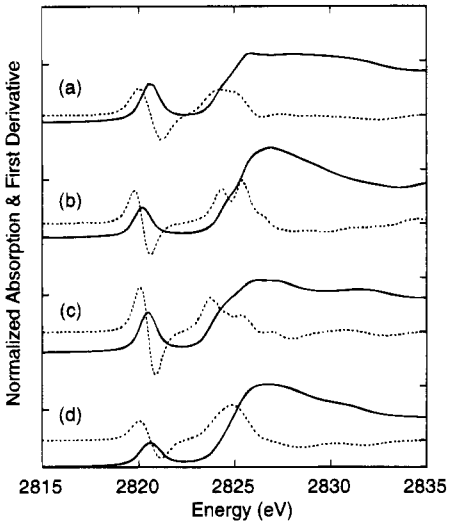

Figure 4. Cl K-edge spectra of the monomeric complexes (a) D_{4h} $CuCl_4^{2-}$, (b) D_{2d} $CuCl_4^{2-}$, (c) square planar *trans*-$CuCl_2pdmp_2$, and (d) square pyramidal $CuCl_5^{3-}$. For each spectrum the solid line is the normalized X-ray absorption data and the dashed line is the first derivative of the data. Each spectrum exhibits a single pre-edge feature well separated from the rising edge. The energy of the feature in spectrum b is lower (2820.2 eV) than those in spectra a, c, and d for which the feature appears at 2820.6, 2820.5, and 2820.6 eV, respectively.

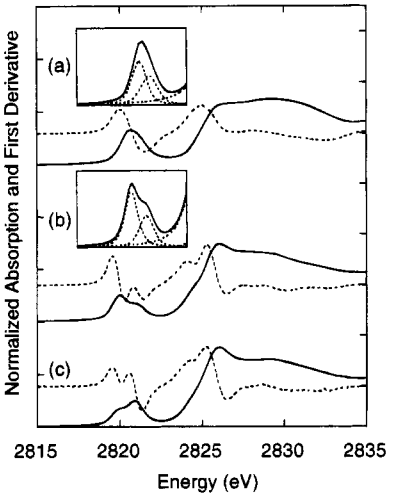

Figure 5. Cl K-edge spectra of dimeric complexes (a) planar $KCuCl_3$, (b) distorted tetrahedral $(Ph_4P)CuCl_3$, and (c) distorted tetrahedral $(Ph_4P)CuClBr_2$. For each spectrum the solid line is the normalized X-ray absorption data and the dashed line is the first derivative of the data. Spectrum a exhibits an asymmetric pre-edge feature; spectra b and c exhibit a split pre-edge feature. Insets a and b show the fit to the pre-edge for $KCuCl_3$ and for $(Ph_4P)CuCl_3$, respectively.

2830.5, and 2824.8 eV for $NaClO_4$, $KClO_3$, and KCl, respectively, reflect these changes due to relative core shifts.

A more realistic charge on the Cl for these compounds has been experimentally estimated using Auger spectroscopy.[31] The charge on the Cl in KCl, $KClO_3$, and $KClO_4$ was determined to be −0.87, +1.49, and +1.91, respectively.[31] While the number of charges which have been experimentally determined are limited, previous studies[11-13] have demonstrated that the relationship between the X-ray edge position and a quantity called the "coordination charge"[32] is linear. Thus, using the charges from the Auger study and the experimental rising edge inflection points, a linear fit to the data in Figure 8 is obtained with $q = -916.66 + 0.32425\ eV^{-1}\ (x)$, where q is the charge on the Cl and x is the rising edge inflection point in eV. This equation can be applied to the Cl 1s → 4p rising edge inflection point for each Cl—Cu(II) complex to obtain an estimate of the charge on the Cl. Table 1 shows the results from such an analysis for complexes with only one type of Cl. For D_{4h}

(31) Nefedov, V. I.; Yarzhemsky, V. G.; Chuvaev, A. V.; Trishkina, E. M. *J. Electron Spectrosc. Relat. Phenom.* **1988**, *46*, 381−404.

(32) The "coordination charge" is given by $\eta = Z - \Sigma_k n_k c_k$ where η is the coordination charge, Z is the formal oxidation state of the absorber, and c_k is the degree of covalency for the kth ligand and n_k is the total number of ligands. Previous studies have used differences in electronegativities to calculate the c_k values (see refs 11−13).

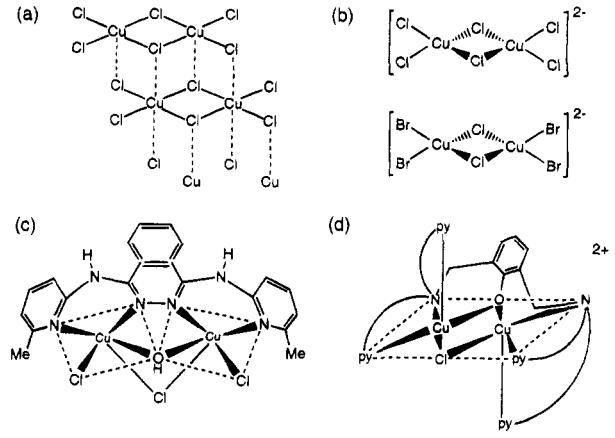

Figure 6. Schematic structures of Cl—Cu(II) dimeric complexes (a) $KCuCl_3$, (b) $(Ph_4P)CuCl_3$ and $(Ph_4P)CuClBr_2$, (c) Cu_2PAP, and (d) $Cu_2(L\text{-}O^-)Cl$.

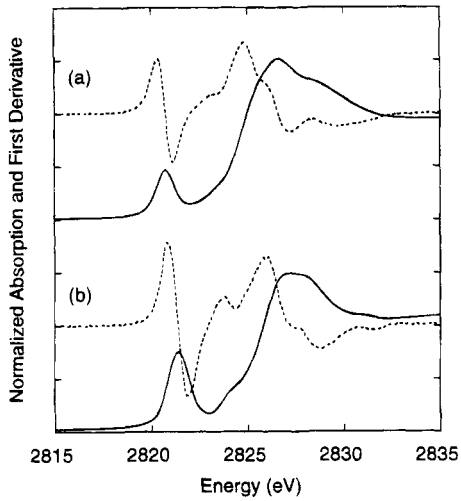

Figure 7. Cl K-edge spectra of dimeric complexes (a) Cu_2PAP and (b) $Cu_2(L\text{-}O^-)Cl$. For each spectrum the solid line is the normalized X-ray absorption data and the dashed line is the first derivative of the data. The pre-edge feature in spectrum a appears at 2820.7 eV while that in spectrum b appears 0.7 eV higher at 2821.4 eV. In addition, the rising edge inflection point is at higher energy for spectrum b and the pre-edge intensity is greater for spectrum b.

$CuCl_4^{2-}$ the charge on each chloride is −0.65, while in D_{2d} $CuCl_4^{2-}$ and $CuCl_2pdmp_2$ it is −0.56. For the bridging chloride in $Cu_2(L\text{-}O^-)Cl$ the charge is −0.39.

For complexes with more than one type of Cl, each may have a distinct core energy which can give rise to different rising edge inflection points. In $CuCl_5^{3-}$ and Cu_2PAP, the axial chlorides (Cl_{ax}) have a significantly weaker bonding interaction with the Cu, and thus the equatorial chlorides (Cl_{eq}) have deeper core energies. Thus, the highest energy maximum in the first derivative reflects the 1s → 4p transition for the Cl_{eq} in each case. Further, the stoichiometry of each site would indicate that the Cl_{eq} should dominate the rising edge region. Thus, the rising edge inflection point for these spectra can be used to calculate the charge on the Cl_{eq} in each case. In $CuCl_5^{3-}$ the Cl_{eq} charge is −0.69 and in Cu_2PAP it is −0.72. These results are given in Table 1.

For the $Cu_2Cl_6^{2-}$ dimers, both the terminal (Cl^t) and bridging (Cl^b) chlorides have strong interactions with the coppers and the Cl 1s → 4p transitions are unresolved. In order to determine which Cl gives rise to the main edge transition (and the corresponding inflection point) a comparison can be made to the Cu_2PAP and $Cu_2(L\text{-}O^-)Cl$ dimers in which the rising edge inflection reflects Cl^t and Cl^b, respectively. The rising edge

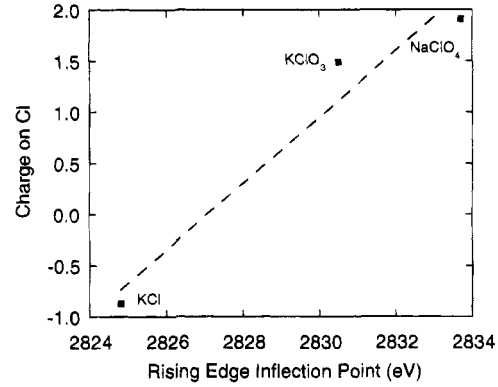

Figure 8. Inflection point of the rising edge of Cl K-edge data plotted *vs* the charge on the Cl determined by Auger spectroscopy for the complexes $NaClO_4$, $KClO_3$, and KCl. The quantitative relationship between the rising edge energy and its total charge is determined by a linear fit to the data points, given by the equation $q = -916.66 + 0.32425\ eV^{-1}(x)$, where q is the charge on the Cl and x is the edge inflection point in eV.

inflection point occurs at (see Table 1) 2824.8 eV for Cl^t in Cu_2PAP and at 2825.8 eV for Cl^b in $Cu_2(L\text{-}O^-)Cl$. The main edge inflection in the planar $KCuCl_3$ dimer is at 2824.9 eV. This inflection point is thus assigned to the Cl 1s → 4p transition for Cl^t. From the stoichiometry of these dimers (2:1 Cl^t:Cl^b), the Cl^t would be expected to make a stronger contribution to the rising edge region. To obtain an estimate for unresolved Cl^b 1s → 4p transition in this spectrum, the magnitude of the pre-edge splitting can be used. While the difference in the Cl^t and Cl^b 1s → 4p transitions is not necessarily the same as the 1s core energy difference (reflected in the pre-edge splitting), the pre-edge splitting of ~0.7 eV provides a useful approximation. Thus, the inflection point for Cl^b would be expected at ~2825.6 eV (given in parentheses in Table 1), consistent with the inflection point for the Cl^b of $Cu_2(L\text{-}O^-)Cl$. The charges which correspond to these inflection points are −0.69 and −0.46 eV for Cl^t and Cl^b, respectively (see Table 1). It should be noted that if the opposite assignment is made (such that the main edge inflection originates from Cl^b), unreasonable values for the charges on each Cl are obtained.

By analogy, the main edge inflection point (at 2825.3 eV) in the tetrahedrally distorted $(Ph_4P)CuCl_3$ can be assigned as corresponding to Cl^t. The unresolved Cl^b inflection point is estimated to be ~1 eV higher at 2826.3 eV (given in parentheses in Table 1). The charges calculated from these inflection points are −0.56 for Cl^t and −0.23 for Cl^b. Due to the uncertainty in obtaining the inflection for Cl^b in these $Cu_2Cl_6^{2-}$ dimers (in addition to the uncertainty in the pre-edge splitting for $KCuCl_3$), the charge on each Cl^b is not rigorously determined.

For systems in which the charges on all ligands are quantitated by the above method, the charge on the central copper can be estimated. For D_{4h} $CuCl_4^{2-}$ each Cl carries a charge of −0.65 and the Cu carries a charge of +0.60. In D_{2d} $CuCl_4^{2-}$ each Cl carries a charge of −0.56 and the Cu carries a charge of +0.24. In the planar dimer $KCuCl_3$, the Cl^t's and Cl^b's carry charges of −0.69 and −0.46, respectively, and each Cu is characterized by a charge of +0.84. In the tetrahedrally distorted dimer $(Ph_4P)CuCl_3$ the Cl^t's and Cl^b's carry charges of −0.56 and −0.23, respectively, which results in a charge on Cu of +0.35. These results indicate that, upon distortion from planarity, the total charge donation to the copper is increased. Further, while each Cl^b in a dimer donates more charge than the Cl^t, each copper in a dimer is more positive than in the analogous monomer because each bridging chloride must donate charge to two metal centers.

Table 2. Cl K-Edge Energy Analysis Parameters

complex	pre-edge energy (eV)[a]	rising edge inflection point (eV)	Cl 1s core energy shift (eV)[b]	ligand field $d_{xy} \rightarrow d_{x^2-y^2}$ transition (cm^{-1})	center of ligand field transitions (cm^{-1})	ligand field induced HOMO shift (eV)	corrected pre-edge energy (eV)	d-manifold energy shift (eV)
			relative to D_{4h}			relative to D_{4h}		relative to D_{4h}
D_{4h} $CuCl_4^{2-}$	2820.6	2825.0	0	12500[e]	14445	0	2820.6	0
D_{2d} $CuCl_4^{2-}$	2820.2	2825.3	−0.3		7100[f]	−0.9[c]	2820.8 ± 0.1	0.2 ± 0.1
$CuCl_2pdmp_2$	2820.5	2825.3	−0.3		9950[g]	−0.6[d]	2820.8 ± 0.3	0.2 ± 0.3
$CuCl_5^{3-}$ (Cl_{eq})	2820.6	2824.9	+0.1	11000[h]		≥−0.2[c]	2820.9 ± 0.1	≥0.3 ± 0.1
$KCuCl_3$ (Cl^t)	2820.6 ± 0.05	2824.9	+0.1	11850[h]		−0.1*c*	2920.8 ± 0.2	0.2 ± 0.2
$KCuCl_3$ (Cl^b)	2821.3 ± 0.09	(2825.6)	(−0.6)					
$(Ph_4P)CuCl_3$ (Cl^t)	2820.0	2825.3	−0.3		10565[i]	−0.5[d]	2820.2 ± 0.3	−0.4 ± 0.3
$(Ph_4P)CuCl_3$ (Cl^b)	2821.0	(2826.3)	(−1.3)					
			relative to $CuCl_5^{3-}$			relative to $CuCl_5^{3-}$		relative to $CuCl_5^{3-}$
$CuCl_5^{3-}$ (Cl_{eq})	2820.6	2824.9	0		11250[h]	0	2820.6	0
Cu_2PAP	2820.7	2824.8	+0.1		14800[i]	+0.4[d]	2820.4 ± 0.3	−0.2 ± 0.3
$Cu_2(L\text{-}O^-)Cl$	2821.4	2825.8	−0.9		14935[k]	+0.5[d]	2820.0 ± 0.3	−0.6 ± 0.3

[a] Error is less than 0.009 unless otherwise noted. [b] Error for these energy differences is estimated to be ±0.1 eV. [c] Shifts are quantitated by differences in the $xy \rightarrow x^2 - y^2$ transition energy. [d] Shifts are quantitated by differences in the centers of the d−d optical transitions for which the uncertainty is ~0.2 eV. [e] Hitchman, M. A. *J. Chem. Soc., Chem. Commun.* **1979**, 973−974. [f] Ferguson, J. *J. Chem. Phys.* **1964**, *40*, 3406−3410. [g] Reference 17. [h] Reference 33. [i] Reference 38. [j] Reference 21. [k] Reference 22.

B. Pre-edge Peak Intensities. As described in the Introduction, the intensity of the pre-edge feature in Cl K-edge spectra of Cl−Cu(II) systems provides a direct probe of the ligand contribution to the HOMO due to bonding.[8]

For symmetrically inequivalent chlorides, only those which contribute Cl 3p character to the HOMO can reflect pre-edge intensity. Therefore, in order to accurately compare the pre-edge intensity for $CuCl_5^{3-}$ and Cu_2PAP to that of the other complexes, the pre-edge intensity must be renormalized. The HOMO is $d_{x^2-y^2}$ for both $CuCl_5^{3-}$ [33] and Cu_2PAP.[34] As the axial chloride of the square pyramid has no overlap with the $d_{x^2-y^2}$ orbital, it cannot contribute to the intensity of the pre-edge feature. Thus, in $CuCl_5^{3-}$, while all five chlorides contribute to the edge jump, only the four equatorial chlorides contribute to the pre-edge intensity. In Cu_2PAP, three chlorides contribute to the edge jump, but only the two equatorial Cl^t contribute to the pre-edge intensity. Further, for systems in which there are more than one pre-edge transition (*e.g.*, both Cl^t and Cl^b transitions), each transition intensity must be renormalized to the total of that type of Cl in the complex. Table 1 gives the renormalized pre-edge intensity for each complex.

The covalency of the Cl−Cu(II) interaction has been determined for D_{4h} $CuCl_4^{2-}$ by a variety of spectroscopic methods.[35] These give a HOMO with 9.8% Cl 3p character donated by each of the four chlorides. Using this value as a calibration of the Cl K-edge pre-edge intensity, the covalency can be calculated from the experimental intensity for each complex using eq 1. The Cl covalency in the HOMO of these complexes ranges from 7.3% per chloride in D_{2d} $CuCl_4^{2-}$ to 13.8% for the Cl^b in $Cu_2(L\text{-}O^-)Cl$. These results are summarized in Table 1.

C. Pre-edge Peak Energies. In order to understand the trends exhibited in the energies of ligand pre-edge features, the separate contributions to the pre-edge energy (see Figure 2) from the Cl 1s core and the HOMO (both ligand field effects and d-manifold shifts) must be quantitated.

The contribution to the pre-edge energy from the Cl 1s core can be determined from the rising edge inflection point of Cl K-edge spectra. As described above, the energy position of the rising edge inflection point gives a measure of the relative Cl 1s core shift. The Cl 1s core energies for each complex relative to D_{4h} $CuCl_4^{2-}$ for four-coordinate complexes and relative to $CuCl_5^{3-}$ for five-coordinate complexes are summarized in Table 2. Because an increase in the coordination number would be expected to raise the overall d-manifold energy, this variable is eliminated if complexes with the same coordination number are compared (*vide infra*).

Energy shifts in the HOMO which are related to variations in ligand field geometry can be taken into account by comparison of the optical d−d transition energies. For structural perturbations which change the geometry of the site only with respect to the ligands in the equatorial plane, changes in the energy of the $xy \rightarrow x^2 - y^2$ optical transition give the relative repulsion of the HOMO. In complexes for which the ligand field transitions have been assigned by polarized single-crystal absorption spectroscopy, comparison of the energies of the $xy \rightarrow x^2 - y^2$ transition can be made.

As the ligand field changes, all orbitals change energy. However, the center of the four fully occupied d-orbitals will experience a more limited change.[36] Thus, a change in the energy center of the ligand field transitions primarily reflects shifts in the HOMO. In cases for which optical assignments have not been made, the shift in the center of the d−d transitions provides a reasonable approximation to the shift in the HOMO. This method introduces a larger uncertainty (~0.2 eV) than the use of assigned d−d transitions. Table 2 summarizes the shifts in the HOMO energy due to ligand field effects relative to D_{4h} $CuCl_4^{2-}$ for four-coordinate complexes and relative to $CuCl_5^{3-}$ for five-coordinate complexes.

These relative energy shifts in the Cl 1s core and the HOMO can be used to obtain pre-edge energies which have been ligand field and core shift corrected. Shifts in the HOMO energy due to ligand field effects are subtracted from and the core 1s energy are added to the observed pre-edge transition energy (see Figure 2). These corrected pre-edge energies are given in Table 2. For cases in which these are the only contributions to the pre-edge energy, the corrected energy will be 2820.6 eV, the pre-edge energy for both D_{4h} $CuCl_4^{2-}$ and $CuCl_5^{3-}$, which have been used as the reference compounds for four- and five-coordinate complexes, respectively. Deviations from this value indicate that an additional effect, the overall energy of the

(33) Desjardins, S. R.; Wilcox, D. E.; Musselman, R. L.; Solomon, E. I. *Inorg. Chem.* **1987**, *26*, 288−300.
(34) Mandal, S. K.; Woon, T. C.; Thompson, L. K.; Newlands, M. J.; Gabe, E. J. *Aust. J. Chem.* **1986**, *39*, 1007−1021.
(35) Solomon, E. I. *Comments Inorg. Chem.* **1984**, *3*, 227−320.
(36) Solomon, E. I.; Hare, J. W.; Dooley, D. M.; Dawson, J. H.; Stephens, P. J.; Gray, H. B. *J. Am. Chem. Soc.* **1980**, *102*, 168−178.

d-manifold, must be taken into account. Table 2 (last column) gives the relative deviation in the corrected pre-edge energy (from 2820.6 eV), which is attributable to a d-manifold energy shift.

D. Correlations in Cl−Metal Bonding. Having defined the information content of Cl pre-edge energies and intensities, one can now use these to obtain insight into bonding differences in related compounds.

***D*$_{4h}$ $CuCl_4^{2-}$ and *D*$_{2d}$ $CuCl_4^{2-}$.** Comparison of the Cl K-edge spectra for D_{4h} $CuCl_4^{2-}$ and D_{2d} $CuCl_4^{2-}$ (Figure 4) shows that the intensity of the D_{2d} complex is lower than that for D_{4h}. The intensity corresponds to a 9.8% covalent contribution to the HOMO per Cl in D_{4h} $CuCl_4^{2-}$, while the covalency of the D_{2d} $CuCl_4^{2-}$ HOMO is 7.3% per Cl (Table 1). As described previously, this is due to the differences in overlap between the Cl 3p orbitals and the Cu $d_{x^2-y^2}$ orbital in the two geometries.[8,9] The D_{4h} Cu $d_{x^2-y^2}$ orbital lobes point directly at the Cl ligands, resulting in higher covalency.

The pre-edge transition energy is 0.4 eV lower for the D_{2d} complex relative to D_{4h} $CuCl_4^{2-}$. While this shift has previously[9] been attributed simply to the effect of the ligand field change, the energy analysis shows that this is a result of a ligand field induced HOMO shift to lower energy in D_{2d} by −0.9 eV in addition to a shift in the D_{2d} 1s core to deeper energy by −0.3 eV. A small energy effect of 0.2 ± 0.1 eV, attributable to a shift to higher energy of the d-manifold of D_{2d} $CuCl_4^{2-}$, emerges from the analysis (Table 2). An overall shift up in the energy of the d-manifold is consistent with a slightly less positive Cu ion in the D_{2d} complex due to more total charge donation by its Cl ligands. The estimated charge on the copper in D_{4h} $CuCl_4^{2-}$ is +0.60 and in D_{2d} $CuCl_4^{2-}$ is +0.24.

This effect of charge donation is further supported by the Cl K-edge spectra which show that the rising edge inflection point is 0.3 eV higher in the D_{2d} complex (Table 1). The relative energy of the rising edge inflection point indicates that the overall charge donation by the Cl in D_{2d} is greater, resulting in a Cl 1s core at deeper binding energy. This is also in agreement with results from a PES study[37] of these complexes which found that D_{2d} $CuCl_4^{2-}$ was characterized by ~3% more Cl covalency over the d-manifold than D_{4h} $CuCl_4^{2-}$. Thus, even though the HOMO for the D_{4h} complex has a higher covalent contribution from Cl, the distortion from planarity in D_{2d} $CuCl_4^{2-}$, which results in slightly shorter bond lengths, allows a more favorable *overall* bonding interaction between the Cl and the copper.

***D*$_{4h}$ $CuCl_4^{2-}$ and $CuCl_2$pdmp$_2$.** The Cl K-edge spectrum of $CuCl_2$pdmp$_2$ (Figure 4) exhibits nearly the same pre-edge intensity as D_{4h} $CuCl_4^{2-}$. The intensity corresponds to 9.7% per Cl in $CuCl_2$pdmp$_2$ (compared to 9.8% in the D_{4h} complex) (Table 1). This indicates that, with respect to the Cu $d_{x^2-y^2}$ orbital, each Cl in $CuCl_2$pdmp$_2$ undergoes a very similar bonding interaction as in D_{4h} $CuCl_4^{2-}$.

The pre-edge transition energy is 0.1 eV lower in the $CuCl_2$pdmp$_2$ complex, and the ligand field shifts the HOMO to lower energy by 0.6 eV. Combined with the core shift to higher energy by 0.3 eV, the energy analysis indicates that the d-manifold is shifted up in $CuCl_2$pdmp$_2$ by 0.2 ± 0.3 eV (Table 2). We are limited in this case primarily by the error associated with the measurement of the ligand field shift of the HOMO. Thus, within the resolution of our analysis there is little significant d-manifold shift in the $CuCl_2$pdmp$_2$ complex relative to D_{4h} $CuCl_4^{2-}$.

The rising edge inflection point is 0.3 eV higher in the $CuCl_2$pdmp$_2$ complex (Table 1), reflecting a core shift to deeper energy by 0.3 eV. This indicates that the overall charge donation by the Cl in $CuCl_2$pdmp$_2$ is larger than that in D_{4h} $CuCl_4^{2-}$. Because two of the negatively charged Cl ligands have been replaced by neutral pyrazoles, each remaining Cl donates more electron density to the metal than in the tetrachloro complex.

***D*$_{4h}$ $CuCl_4^{2-}$ and $CuCl_5^{3-}$.** The renormalized Cl K-edge pre-edge intensity in $CuCl_5^{3-}$ (Figure 4) is lower than that in D_{4h} $CuCl_4^{2-}$. The $CuCl_5^{3-}$ intensity corresponds to 9.1% per Cl_{eq} in the HOMO (Table 1). In the square pyramidal geometry, the Cu is 0.3 Å above the plane of the four Cl_{eq} ligands. Thus, the Cl_{eq} ligands have less direct overlap with the Cu $d_{x^2-y^2}$ orbital than in the planar D_{4h} $CuCl_4^{2-}$. This change in the geometry, then, slightly decreases the Cl_{eq} covalent contribution to the HOMO.

The observed pre-edge transition energy is the same in both complexes. The shift in the ligand field in $CuCl_5^{3-}$ relative to D_{4h} $CuCl_4^{2-}$ is determined from the energy of the optical $xy \rightarrow x^2 - y^2$ transition, which indicates a shift down of the $CuCl_5^{3-}$ HOMO by at least 0.2 eV due to a decrease in the repulsive interaction of the $x^2 - y^2$ orbital with the equatorial ligands when they are distorted out of the Cu xy plane. In this case the xy orbital may also experience less repulsion. Thus, the absolute shift in the $x^2 - y^2$ orbital may be even larger than 0.2 eV. Combined with the core shift to higher energy by 0.1 eV, the energy analysis indicates that the overall d-manifold is shifted to higher energy in $CuCl_5^{3-}$ by at least 0.3 eV (Table 2). This d-manifold shift is due to the increase in coordination number which increases the repulsive, antibonding interaction experienced by the metal center.

The rising edge inflection point for the Cl_{eq} in $CuCl_5^{3-}$ is 0.1 eV lower than that observed in D_{4h} $CuCl_4^{2-}$, reflecting a core shift to higher energy by 0.1 eV in $CuCl_5^{3-}$. This indicates that the overall charge donation by the Cl_{eq} in $CuCl_5^{3-}$ is slightly less than in D_{4h} $CuCl_4^{2-}$. The equatorial bond lengths in these two complexes are nearly identical (2.250 Å[14] and 2.255 Å[18] for D_{4h} $CuCl_4^{2-}$ and $CuCl_5^{3-}$, respectively). However, the presence of additional Cl_{ax} results in each of the Cl_{eq} ligands donating somewhat less charge than in the four-coordinate complex.

***D*$_{4h}$ $CuCl_4^{2-}$ and $KCuCl_3$.** The planar dimer $KCuCl_3$ exhibits two, unresolved pre-edge features (Figure 5). As prescribed in the Results, the lower energy transition is assigned as originating from Cl^t and the higher energy from Cl^b. The renormalized intensity of Cl^b is somewhat larger than that for Cl^t, corresponding to a covalency per Cl of 12.7 ± 1.8% for Cl^t and 13.5 ± 3.5% for Cl^b. The uncertainty in these measurements, which originates from the overlapping nature of the features, limits our ability to make quantitative comparisons of these covalencies. Both chlorides in the dimer seem to be slightly more covalent with respect to the HOMO than that observed in D_{4h} $CuCl_4^{2-}$.

The Cl^t and Cl^b pre-edge transition energies are separated by approximately 0.7 eV. Because these two transitions are from within the same molecule, the HOMO energy is fixed. Thus, this energy splitting provides a *direct* measure of the difference in the Cl 1s core energies. The splitting is a clear indication that each Cl^b, which is bound to two coppers, donates more negative charge than each Cl^t, which is bound to only one copper. This causes the Cl^b 1s core orbital to shift to deeper binding energy and results in a pre-edge transition at higher energy.

(37) Didziulis, S. V.; Cohen, S. L.; Gewirth, A. A.; Solomon, E. I. *J. Am. Chem. Soc.* **1988**, *110*, 250−268.

The Cl^t pre-edge transition energy in $KCuCl_3$ is the same as that in D_{4h} $CuCl_4^{2-}$, while the Cl^b transition is ~0.7 eV higher. The shift in the HOMO due to shifts in the ligand field for $KCuCl_3$, relative to D_{4h} $CuCl_4^{2-}$, is calculated to be −0.1 eV from the $xy \rightarrow x^2 - y^2$ transition. Combined with the core shift to higher energy by 0.1 eV for the Cl^b (relative to D_{4h} $CuCl_4^{2-}$), this indicates that the overall d-manifold is shifted to higher energy in $KCuCl_3$ by 0.2 ± 0.2 eV (Table 2). Thus, within the resolution of our analysis, there is no net d-manifold shift in the dimer relative to the square planar monomer.

As described previously, the total charge on the Cu (+0.84) is more positive in the dimer than in the D_{4h} monomer (+0.60). Thus, while each Cl^b donates more total charge than a Cl^t, the total charge donation to each copper is less in the dimer than in the monomer. This change in charge would cause the copper orbitals to be shifted to lower energy in the dimer. However, due to the weak axial interactions in this complex the coordination number is increased from 4 to 6 (tetragonally elongated), increasing the repulsive interaction of the d-orbitals with the ligands. These two effects, which result in opposing d-manifold shifts, combine to give little net change in the d-manifold energy.

The rising edge inflection point reflects a core shift to lower binding energy by ~0.1 eV in the Cl^t of $KCuCl_3$ relative to the Cl in D_{4h} $CuCl_4^{2-}$. By comparison of the pre-edge transition splitting, the Cl^b core is estimated to be ~0.6 eV to lower energy than in D_{4h} $CuCl_4^{2-}$. This indicates that the overall charge donation by the Cl^t in $KCuCl_3$ is similar to the Cl in D_{4h} and the donation by Cl^b is greater due to the interaction with two coppers.

D_{4h} $CuCl_4^{2-}$ and $(Ph_4P)CuCl_3$. The distorted tetrahedral dimer $(Ph_4P)CuCl_3$ also exhibits two resolved pre-edge features. As described in the Results, the lower energy transition originates from Cl^t and the higher energy from Cl^b. The renormalized intensity of Cl^b is larger than that for Cl^t, corresponding to a covalency per Cl of 9.5% for Cl^t and 11.7% for Cl^b (Table 1). These results clearly indicate that the Cl^b undergoes a more covalent interaction with respect to the HOMO due to its bonding to two coppers. The value of the Cl^t covalency is only slightly less than the 9.8% per Cl for D_{4h} $CuCl_4^{2-}$. While distortion toward T_d in the D_{2d} $CuCl_4^{2-}$ monomer reduced the Cl HOMO covalency, the distortion from planarity in this dimer complex is not as large. Further, the Cu—Cl^t bond length is significantly shorter in the $(Ph_4P)CuCl_3$ dimer than in D_{4h} $CuCl_4^{2-}$ (2.192[20,38] *vs* 2.250 Å,[14] respectively) which will serve to increase the covalent interaction. This combination of factors results in only a small total reduction in covalency for Cl^t relative to D_{4h} $CuCl_4^{2-}$.

The Cl^t and Cl^b pre-edge transition energies are separated by 1.0 eV. As in the planar dimer, this energy splitting provides a *direct* measure of the difference in the Cl 1s core energies. The splitting is a clear indication that Cl^b donates more overall charge in the dimer through its interactions with two coppers.

The pre-edge transition energy is 0.6 eV lower for the Cl^t, and transition from Cl^b is 0.4 eV higher than in D_{4h} $CuCl_4^{2-}$. The shift in the ligand field in $(Ph_4P)CuCl_3$, as calculated from the centers of the optical d−d transitions, indicates a shift down of the HOMO in $(Ph_4P)CuCl_3$ by 0.5 eV relative to D_{4h} $CuCl_4^{2-}$, which would be expected for the distortion away from planarity. Combined with the core shift to deeper energy by 0.3 eV for Cl^t, this indicates that the overall d-manifold is shifted to lower energy in $(Ph_4P)CuCl_3$ by 0.4 ± 0.3 eV (Table 2). This is consistent with a higher positive charge on the copper, which would result in a shift of all Cu orbitals to lower energy. However, the charge calculated above for the coppers in this dimer (+0.35) is less positive than the Cu (+0.60) in D_{4h} $CuCl_4^{2-}$. Because this calculated charge depends on an indirect estimate of the Cl^b core shift, the above d-manifold shift indicates that this approximation overestimates the total charge donated by Cl^b in this complex.

The rising edge inflection point in $(Ph_4P)CuCl_3$ corresponding to Cl^t appears 0.3 eV higher than the Cl in D_{4h} $CuCl_4^{2-}$ and reflects a core shift to deeper energy by 0.3 eV in Cl^t. From the pre-edge transition splitting, then, the Cl^b core is shifted to ~1.3 eV to deeper energy than in D_{4h} $CuCl_4^{2-}$. This indicates that the overall charge donation by Cl^t in $(Ph_4P)CuCl_3$ is slightly more than that by the Cl in D_{4h}, and the donation by Cl^b is significantly greater. The increased charge donation by Cl^t is due to the change in geometry which, as in the D_{2d} monomer, favors an increase in the overall charge donation by the ligands. The shorter Cl^t—Cu(II) bond length also allows for a relative increase in the Cl^t charge donation. Relative to Cl^t, the increase in charge donation by Cl^b is again due to its interaction with two coppers.

Cu_2PAP and $Cu_2(L\text{-}O^-)Cl$. The Cu_2PAP and $Cu_2(L\text{-}O^-)Cl$ dimers contain square pyramidal coppers with N/O coordination. Each Cu in Cu_2PAP has one terminal Cl_{eq} which contributes to the pre-edge feature, while the two coppers in $Cu_2(L\text{-}O^-)Cl$ are bridged by a single equatorial chloride.

The renormalized pre-edge intensity is significantly higher for $Cu_2(L\text{-}O^-)Cl$ than for Cu_2PAP (Figure 7). This corresponds to 13.7% covalent contribution per Cl in $Cu_2(L\text{-}O^-)Cl$ and a 10.1% covalent contribution per Cl in Cu_2PAP. The high covalency in $Cu_2(L\text{-}O^-)Cl$ is due to the bridging nature of the chloride bonding interaction.

The Cu_2PAP Cl_{eq} can be compared to the Cl_{eq} in $CuCl_5^{3-}$. The covalent contribution to the HOMO of each Cl_{eq} in Cu_2PAP is higher than that in $CuCl_5^{3-}$ (9.1%), which is likely due to the significant distortion of the square pyramid in Cu_2PAP[30] resulting in a more favorable $d_{x^2-y^2}$—Cl 3p interaction than in $CuCl_5^{3-}$.

In contrast to observations for the monomeric $CuCl_2pdmp_2$, there is no indication that the chlorides in these dimers donate more total charge due to the substitution of N/O ligation at the copper sites. This is likely due to the variations in donating ability by these ligands which, due to the complexity of the ligands, can not be easily determined.

The pre-edge energy for Cu_2PAP is 0.7 eV lower than in $Cu_2(L\text{-}O^-)Cl$. As the energy analysis in Table 2 shows, the relative 1s core energies for the chlorides in these dimers are different by 1.0 eV, while the ligand field contributions to the HOMO energies are nearly the same. Thus, a small difference in the overall d-manifold is indicated which can likely be attributed to differences in bonding interactions with the non-chloride ligands.

The difference between the rising edge inflection points, 2824.8 and 2825.8 eV for the terminal Cl_{eq} of Cu_2PAP and the Cl^b of $Cu_2(L\text{-}O^-)Cl$, respectively, clearly illustrates the difference in charge donation by the terminal and bridging chloride. Cl^b donates significantly more charge due to its interaction with two coppers which shifts the Cl^b 1s core to deeper energy.

Discussion

Ligand K-edge spectroscopy has been shown to be a powerful tool in the study of the electronic structure of metal-ligand interactions. The intensities of pre-edge features provide a direct probe of the covalent contribution of the ligand to the HOMO orbital. The energies of these pre-edge features can be corrected for ligand field effects and shifts in ligand core energy to reveal the relative energy of the d-manifold of the metal in the complex.

(38) Willett, R. D.; Chow, C. *Acta Crystallogr.* **1974**, *B30*, 207−214.

Finally, the rising edge inflection point energy reflects the Cl 1s core energy and can be related to the relative charge donated by the ligand in the complex.

Results obtained from the application of this methodology to several systems are strongly supported by independent spectral data or by basic ligand field concepts. The d-manifold shift to less deep binding energy in D_{2d} *vs* D_{4h} $CuCl_4^{2-}$ indicates the Cu in the D_{2d} complex is less positively charged. This result is supported by PES studies[37] which showed the D_{2d} complex to be more covalent over its orbitals than the D_{4h} complex. Further, this study indicates a shift up in the d-manifold energy for square pyramidal $CuCl_5^{3-}$ relative to D_{4h} $CuCl_4^{2-}$ when a fifth ligand is added to the coordination sphere. This is supported by basic ligand field concepts which give the average d-orbital energy to be proportional to, $\sum_i Z_i e/a$, which is a sum over i ligands with a metal−ligand distance of a and charge Z_i.[39]

The application of energy and intensity models to a series of Cl—Cu(II) complexes has allowed us to define the chemical basis for effects which contribute to pre-edge energies and intensities.

In a geometric distortion from a square planar to a distorted tetrahedral structure, a decrease in the covalent Cl contribution to the HOMO and an increase in the overall charge donation by Cl ligands are observed. The results show clearly that while the geometry can maximize the overlap and result in a high covalency in the HOMO, this is not necessarily reflective of the overall charge donation. However, because the half-occupied HOMO serves as the redox-active orbital in Cu(II) systems, the covalency of this orbital is crucial for understanding the catalytic properties of Cu in enzymatic systems.

The bonding interaction with copper is very different for terminal *vs* bridging chlorides. Due to the interaction with two copper ions, bridging chlorides donate more total charge than terminal chlorides. This difference in bonding is also reflected in a relatively larger covalent contribution to the HOMO for bridging chlorides.

An increase in the coordination number or an increase in charge donation by the ligands (resulting in a less positively charged copper ion) has been shown to result in an increase in the overall energy of the d-manifold of the copper.

The Cl—Cu(II) bonding is dependent on the nature of the other coordinating ligands. Replacing chlorides with less strongly donating pyrazoles causes the remaining chlorides to donate more total charge relative to the tetrachloro complex.

Ligand pre-edge features, which contain contributions from both the Cl 1s core and the antibonding HOMO, are more complicated than features localized only on the ligand or metal. However, this study has shown that the different contributions can be separated to provide insight into the ligand—metal interactions of the site.

These studies, which demonstrate how ligand K-edge X-ray absorption features can be used to obtain information about ligand—metal bonding, form the basis for future ligand XAS studies. In particular, this methodology can be applied to study the differences in covalency of S(Cys)—Cu(II) bonding interactions and the relationship to electron transfer reactivity in perturbed blue copper sites. Further, the fact that ligand K-edge XAS can resolve features of bridging and terminal chlorides will be important for studies on iron−sulfur metalloproteins, in which the active site contains bridging inorganic sulfide as well as terminal cysteine sulfur ligands.

Acknowledgment. This research was supported by Grants RR-01209 [NIH] and CHE-9121576 [NSF] (K.O.H.) and Grants CHE-9217628 [NSF] (E.I.S.). SSRL operations are funded by the Department of Energy, Office of Basic Energy Sciences. The Biotechnology Program is supported by the NIH, Biomedical Research Technology Program, National Center for Research Resources. Further support is provided by the Department of Energy, Office of Health and Environmental Research. The authors also thank Prof. Kenneth Karlin for providing the precursor to $Cu_2(L\text{-}O^-)Cl$ and Dr. William Estes for helpful discussions about the synthesis of $(Ph_4P)CuClBr_2$.

(39) Figgis, B. N. *Introduction to Ligand Fields*; John Wiley & Sons, Inc.: New York, 1966, p 31.